

## Hillock formation on ion-irradiated graphite surfaces

K. Nordlund\*

*Accelerator Laboratory, P.O. Box 43, FIN-00014 University of Helsinki, Finland*

T. Mattila

*Laboratory of Physics, Helsinki University of Technology, FIN-02150 Espoo, Finland*

(December 31, 1996)

Scanning probe microscopy experiments show that ion irradiation of (0001) graphite results in the formation of isolated defects comprising of a few tens of atoms. We use molecular dynamics simulations and density-functional theory calculations to study the formation probabilities of these defects. We identify different defect structures which correspond to experimentally observed hillocks on graphite surfaces. We find that the predominant source of defects are vacancies and interlayer interstitials, and identify a three-atom carbon ring defect on the graphite surface.

68.35.Dv, 34.20.Cf, 61.80.Jh

### I. INTRODUCTION

Many aspects of ion irradiation-induced effects on graphite surfaces have been subject to much interest recently [1–6]. Despite the extensive experimental work it is still to some extent unclear what atomic structures and formation mechanisms are the source of observed damage structures.

The crystal structure of graphite is peculiar in that the atoms are ordered in planar layers where the separation between the layers (3.35 Å) is almost 2.5 times the nearest-neighbour distance within the layers (1.42 Å) [7]. Within the planar layers, the carbon atoms are ordered in a hexagonal “honeycomb” structure. The atoms within the layers have strong covalent  $sp^2$  bonding, whereas there is only a very weak residual bonding between the layers.

Scanning tunneling microscopy (STM) and atomic force microscopy (AFM) measurements of graphite surfaces damaged by low-dose ion irradiation have shown that the defects formed on the surfaces can be roughly divided in two categories: large-scale complex defects, and small-scale defects comprising of a few tens of atoms [5,6,8–10]. The defects in the latter category typically appear as hillocks (bumps) in which the atomic structure appears unmodified, but has risen 1 – 10 Å from the surroundings.

Very recently Hahn *et al.* have shown that vacancies on the graphite surface can appear as surface protrusions in STM measurements [5]. Some of the hillocks seen in experiment are caused by impurity atoms between the surface and second layer of atoms in graphite [5,8]. How-

ever, hillocks occur also during self-ion-implantation [11] and one incident atom may cause the formation of several hillocks [6]. Thus, in many cases the formation of hillocks involves only carbon atoms. In this paper, we restrict ourselves to such processes.

Since STM measurements of graphite surfaces show one protrusion in the observed electronic density per two surface atoms, it is difficult to deduce the atomic structure based on experiment alone. Several authors have studied graphite surface erosion processes using MD simulations. R. Smith has simulated several dynamical processes occurring on graphite surfaces (see e.g. [12,13]), and recently Gras-Martí *et al.* have studied the early stages of hillock formation on ion-implanted graphite [14]. To our knowledge, there has been no systematic study on the formation probability and final structure of surface defects.

In this paper, we use molecular dynamics (MD) simulations of collision cascades to study the formation of the small-scale defects, and *ab initio* calculations to study the stability and electronic structure of these defects. We use our recently developed enhancement of the Tersoff potential to include a description of the graphite interlayer forces in the simulations [15]. We collect representative statistics from MD simulations of collision cascades to obtain a quantitative view of the defect formation processes.

### II. PRINCIPLES OF THE CALCULATIONS

Molecular dynamics simulations offer a powerful tool for understanding dynamical processes in materials. Since our objective is to obtain representative statistics from simulations of systems involving several thousands of atoms, quantum or tight binding MD methods [1] are computationally too intensive to suit our purposes.

---

\*Email kai.nordlund@helsinki.fi. Temporary address until April 1997: Materials Research Laboratory, University of Illinois at Urbana-Champaign, Urbana, IL 61801, USA.

In classical MD simulations, it is essential to use a realistic interatomic potential. We have recently developed an interatomic potential for carbon based on the Tersoff potential formulation [16,17]. Our potential essentially adds a long-range weak interaction which treats the inter-plane interactions in graphite, and a repulsive potential obtained from *ab initio* calculations to the well-known Tersoff potential. The long-range potential has its onset at  $r$  values larger than the Tersoff potential high-end cut-off, and the short range potential is fitted to the Tersoff potential using a Fermi function in the repulsive potential region. Therefore, the total potential describes adequately both the long-range interlayer forces in graphite and the repulsive part of the potential, while it retains the good description of ordinary short-range bonding in carbon given by the Tersoff potential. The functional form of our potential is given in Ref. [15].

In our MD simulations, we use the microcanonical formalism and the Smith-Harrison algorithm for the solution of the equations of the motion [18]. A combined linked cell-method and Verlet neighbour list is used for finding neighbouring atoms [19]. To reduce the size of the neighbour lists and the calculation time, we use different neighbour lists for the short range Tersoff potential interactions and the long-range graphite interactions of our potential. Since simulations of collision cascades involve drastic changes in the velocities of the atoms, we use a variable time step scheme to speed up the simulations [20].

The ZBL electronic stopping power [21] is used to treat the inelastic energy loss of all atoms with an energy higher than thermal energies. The simulation cell consists of 2000 - 3000 atoms arranged so that the parts of the collision cascade affecting the surface are contained within the cell borders. The temperature of the atoms near the cell border is scaled down to 300 K during the simulation to dissipate kinetic energy out of the simulation cell. Periodic boundary conditions are employed in the  $x$  and  $y$  directions to model interactions over the simulation cell borders. In the  $z$  direction, the upper boundary condition is left open to model the graphite surface. Since the interactions between graphite planes are weak, and we are interested in phenomena occurring on the surface or between the first and second graphite layer, we found that six graphite layers in the  $z$  direction were enough for the simulations. The atoms in the lowest-level graphite layer are held fixed to model the interlayer interaction from bulk graphite.

At least two hundred recoil events were simulated for each type of initial recoil condition to obtain representative statistics of the defect formation processes. To obtain the equilibrium atomic configuration, the temperature of the simulation cell was quenched down to 0 K after the collision cascade had thermalized. We verified that the defect types produced in the simulations are stable for at least 3000 fs after the thermalization of the

collision cascade and that the quench does not change the defect structure.

In the simulations, collective oscillations in the graphite planes with amplitudes of the order of 0.5 - 1 Å were frequently seen to result from the collision processes. The oscillations continued throughout the picosecond time scale used in the simulations. Since the forces in the  $z$  direction are very weak, the quench was not able to remove all the buckling within a reasonable simulation time.

The defects produced were identified using a separate computer code to analyze the final atomic structure after the quench. The analysis criteria were determined so that the computer analysis yielded the same conclusions as were obtained by inspection of the atomic structure obtained from the simulations. Vacancies were identified by searching for nearby graphite atoms within the top plane with less than three bonds (the number of bonds for atoms in undamaged graphite). Interlayer interstitial atoms were identified as atoms with neighbours not far below and above the atom (due to residual buckling of the layers after the quench, a straightforward analysis of the  $z$  coordinate would not be adequate in all cases). In many cases, interstitial atoms formed a tetrahedral bond structure with atoms in the layer above or below. However, it is well known from experiment that the migration energy for interstitials is very low [22], so we classified the tetrahedral structure as a (mobile) interstitial atom. D3 defects (see below) were identified by looking for two-foldly bonded atoms in the top layer of atoms, where the angle between the bond directions was close to 180° when projected on the  $xy$  plane.

To study the effect of low-energy ion-implantation on defect production, we simulated 100 eV - 3 keV carbon recoils incident on the (0001) graphite surface, aligned 65° from the [0001] axis towards the [0010] axis (cases 1 - 3 in Table I). To study defects formed by secondary recoils in high energy implantations (cf. e.g. Ref. [6]), we simulated secondary recoils with energies 100 eV - 3 keV. These were modeled by placing an extra atom between the third and fourth layer in graphite, and giving it an initial direction towards the surface chosen isotropically in the solid angle cone defined by the [0001] and [0031] crystal directions (cases 4 - 7 in Table I). Although the secondary recoil simulations can not be directly linked to experiment, we believe they still give an indication of the number of defects which may be formed by secondary recoils during high-energy implantation at small angles [6].

STM and AFM measurements do not directly measure the atomic structure, but rather the partial electron density of the uppermost valence electron levels (STM) and the total electron density (AFM) [5]. Therefore, it is desirable to know the electronic structure of surface defects to do a comparison with experiment [23-25].

To study the stability and electronic structures of the defect types we performed DFT/LDA [26] calculations

using the plane-wave pseudopotential method. Principally we employed the Vanderbilt ultra-soft pseudopotentials [27] which provide an efficient way to describe the sharp  $2p$  wavefunctions of the first-row elements. In the case of carbon, a 20 Ry kinetic energy cut-off was found to give well converged results. Supercells containing up to 51 atoms were applied and full atomic relaxations were allowed. As many vacuum layers as occupied atom layers in the  $c$ -axis direction were employed for surface description. For  $k$ -point sampling we used the  $\Gamma$ -point. Test calculations with special  $k$ -points [28], different supercell sizes and norm-conserving pseudopotentials [29] were performed to ensure the reliability of our results.

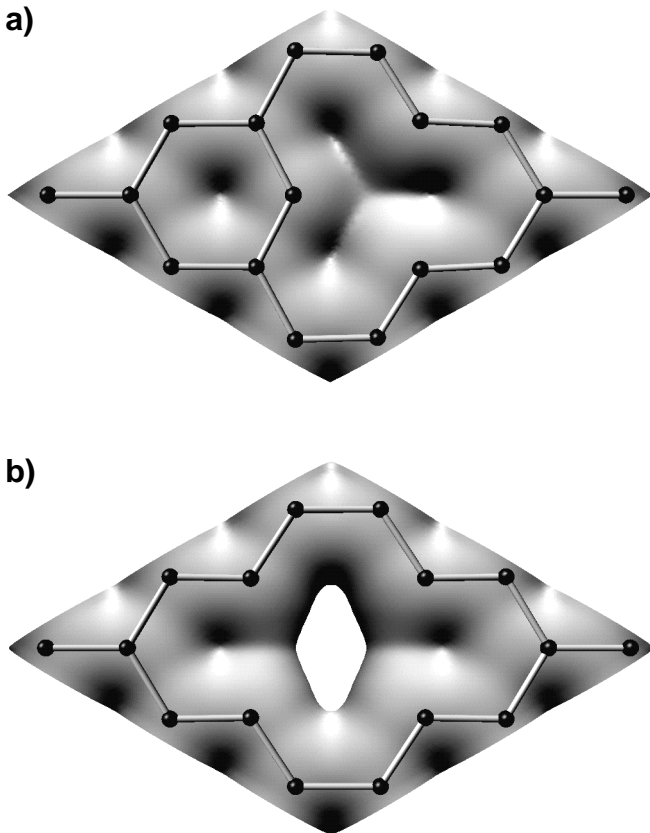


FIG. 1. The total valence electron density associated with a monovacancy (a) and a divacancy (b) in the top-most graphite layer viewed from above. The constant-value surface corresponds to a valence electron density of  $0.02 e/\text{bohr}^3$ . The atoms are superimposed on the electron density surface for clarity.

### III. RESULTS AND DISCUSSION

From our MD simulations we identified three main types of surface defects occurring in statistically signif-

icant number. These were surface vacancies, interplane interstitials below the surface layer and D3 defects. These defect structure types accounted for more than 99 % of all defects produced.

For mono-vacancies, our *ab initio* calculations revealed that no considerable change in the total valence electron density is connected to the missing atom site (Fig. 1 (a)) when compared with the ideal structure. However, we found that the partial charge density which originates from the states close to the Fermi energy is enhanced at the atoms surrounding the vacancy. These results are in a good agreement with those of Hahn *et al.* [5], who state that vacancies are not observable by AFM but appear as protrusions in STM. We also investigated the electronic structure of divacancies. Fig. 1 (b) shows that the total valence electron density above a divacancy is considerably reduced, which is in clear contrast with the case of a mono-vacancy in Fig. 1 (a). However, it is apparent from the measurements by Hahn *et al.* [5] that AFM cannot directly detect even larger vacancies despite the notable changes in the total valence electron density, which supports the low sensitivity of AFM in imaging atomic-scale defects on graphite.

The carbon single interstitial between planes is mobile at room temperature [22] and can therefore not be the source of hillocks. However, single interstitials may migrate to form dimers and clusters between the layers [30], which may be the source of some of the hillocks. Interstitials do not annihilate with vacancies in significant numbers at room temperature [22,30]. Using our interatomic potential we found that an interlayer dimer and trimer produce relatively low and broad hillocks, with atomic heights of 0.7 Å and 1.0 Å, and volumes corresponding to roughly 5 and 14 atomic volumes, respectively. Computer capacity limitations prevented us from studying interstitials using *ab initio* methods.

Since defect migration occurs on relatively long time scales, the formation of clusters can not be simulated using molecular dynamics simulations. However, an upper bound for their number can be obtained by dividing the number of single interstitials by two.

In addition to vacancies and interstitials, we also found a surface defect where an extra atom has entered the top layer. When seen from above, it appears as two carbon rings with seven atoms, while from the side its center appears as a triangle formed by three carbon atoms (Fig. 2). We label this defect type “D3”. The middle atom is about 2 Å higher than the undisturbed lattice, and its neighbouring atoms have risen significantly from the surrounding. The triangle is nearly equilateral, with lengths 1.49 Å for the upward bonds and 1.56 Å for the horizontal bond.

The D3 structure could be considered a form of buckled carbon occurring fully within a graphite layer, having some similarity with the “bowl” structure discussed in Ref. [31]. Also, it bears an interesting likeness to the

three-atom rings which have very recently been suggested to have a significant role in the structure of amorphous carbon [32], and also seen in studies of the formation of fullerenes [33].

The *ab initio* calculations also indicated that the D3 defect structure is stable and gave a binding energy of -3 eV and a formation energy of 7 eV for it (by comparison, the Tersoff potential gave an about 1 eV lower formation energy). Inspection of collision cascades showed that the structure can be formed by a single low-energy ( $E \sim 50$  eV) recoil atom incident on the surface layer from below, displacing an atom in a graphite ring which then enters an interstitial site [34]. Due to the relatively high formation energy and the necessity for an extra atom

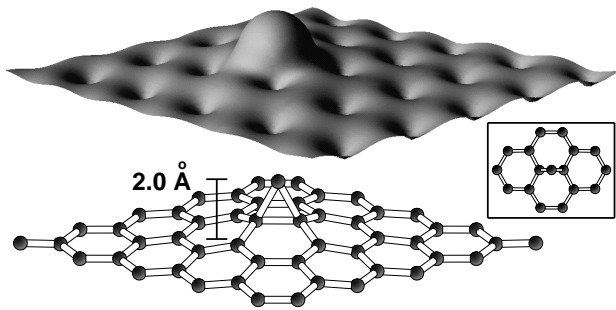


FIG. 2. Atomic and electronic structure of the D3 defect identified in our simulations. The constant-value surface corresponds to a valence electron density of  $0.02 e/\text{bohr}^3$ . To provide a clear view of the atomic structure, the electron density has been raised in the figure. The inset shows the defect viewed from above the graphite (1000) surface.

to break into the very stable graphite layers, we think the formation of the D3 defect requires the presence of strongly non-equilibrium conditions like those in collision cascades.

Both the valence electron density and the partial charge density of the uppermost occupied orbital have strong maxima above the top atom in the defect (Fig. 2), which indicates that the structure appears as a hillock in AFM and STM measurements, with a height of at least 2 Å.

We tested the stability of the D3 defect by simulating a cell containing 1441 atoms including one D3 defect at different temperatures. We found that up to a temperature of 5000 K the defect remained stable at least for 10 ps (the potential underestimates the melting temperature of graphite). Considering that the probability of defect migration or breakup usually reduces as the exponential of the inverse of the temperature, it seems quite possible the defect is stable for long time periods at room temperature. However, since the top atom carbon atom in the D3 defect has only two bonds, we think it is possible it will react chemically if placed in an atmosphere con-

taining reactive atoms (however, we have not attempted any analysis of the probability of such processes).

In Table I we present formation probabilities obtained for the defect types presented above. Note that the figures given in the table are the average number of a certain type of defect produced by one ion, not the formation probability relative to the total number of defects. From the Table, we see that in case of *incident* recoils vacancies and single interstitials occur in roughly equal numbers. Taking into account that single interstitials must form clusters to produce visible hillocks at room temperature, we see that vacancies are the dominant source of hillocks in low-energy ion implantation. The D3 defects account for 0 – 3 % of the observable defects.

TABLE I. Average number of different types of defects produced on the graphite surface by one recoil atom. Cases 1 – 3 denote implantation of a recoil incident on graphite, cases 4 – 7 secondary recoils. N denotes the number of events simulated. SV denotes single vacancies in the graphite surface layer, CV di-, tri-, etc. vacancies and groups of nearby single vacancies and SI single interstitial atoms between the surface and second layer.

Implantation case	N	Defects/recoil atom			
		SV	CV	SI	D3
1. 300 eV inc.	264	0.62	0.15	0.55	0.0
2. 1 keV inc.	255	0.43	0.54	1.14	0.02
3. 3 keV inc.	220	0.63	0.30	0.96	0.04
4. 100 eV sec.	204	0.0	0.0	0.61	0.005
5. 300 eV sec.	309	0.31	0.06	0.74	0.06
6. 1 keV sec.	240	0.46	0.17	0.56	0.02
7. 3 keV sec.	201	0.29	0.11	0.31	0.005

*Secondary* recoils (cases 4 – 7 in the Table) form significantly more single than complex vacancies at all energies. The lower energy secondary recoils (cases 4 and 5) are likely to be stopped within the graphite lattice, and therefore form more interstitial atoms, whereas the higher energy secondary recoils form more vacancies. Again, taking interstitial clustering into account, we see that vacancies are the dominant source of defects. Secondary recoils with energies of a few hundred eV (occurring frequently in cascades formed during high-energy ion implantation) also have a significant contribution of D3 defects. We emphasize that due to the relatively low statistics and the fact that our interatomic potential slightly underestimates the formation energy of the D3 defect, the figures for the formation probabilities of the D3 defect have some degree of uncertainty.

#### IV. CONCLUSIONS

We have studied the formation mechanisms and structures of different types of defects and discussed their correspondence to experimental STM and AFM results. We

found that the predominant source of small-scale hillocks seen in STM measurements are single and complex vacancies and that at most half of the defects may be formed by interstitial atom clusters. We further identified a surface defect in which an extra atom has entered the surface layer which we suggest may be the source of some of the hillocks seen in experiment.

## ACKNOWLEDGMENTS

Prof. W. Bolse is acknowledged for useful discussions about the interpretation of their STM experimental results. One of the authors (T. Mattila) acknowledges financial support by the Vaisala Foundation.

- 
- [1] G. Galli and F. Mauri, Phys. Rev. Lett. **73**, 3471 (1994).
  - [2] R. A. Spits, J. F. Prins, and T. E. Derry, Nucl. Instr. Meth. Phys. Res. B **85**, 347 (1994).
  - [3] L. Begrambekov, S. Vergazov, A. Zakharov, and M. Morochev, Nucl. Instr. Meth. Phys. Res. B **90**, 491 (1994).
  - [4] I. Koponen and M. Hautala, Nucl. Instr. Meth. Phys. Res. B **103**, 156 (1994).
  - [5] J. R. Hahn, H. Kang, S. Song, and I. C. Jeon, Phys. Rev. B **53**, R1725 (1996), and references therein.
  - [6] K. P. Reimann, W. Bolse, U. Geyer, and K. P. Lieb, Europhys. Lett. **30**, 463 (1994).
  - [7] R. Wyckoff, *Crystal Structures*, 2nd ed. (Interscience, New York, 1963), Vol. I, p. 27.
  - [8] D. Marton *et al.*, Surf. Sci. **326**, L489 (1995).
  - [9] R. Coratger *et al.*, Surf. Sci. **262**, 208 (1992).
  - [10] L. Porte *et al.*, Nucl. Instr. Meth. Phys. Res. B **44**, 116 (1989).
  - [11] R. Coratger, A. Claverie, F. Ajustron, and J. Beauvillain, Surf. Sci. **227**, 7 (1990).
  - [12] R. Smith, Proc. Roy. Soc. Lond. A **431**, 143 (1990).
  - [13] R. Smith and R. P. Webb, Nucl. Instr. Meth. Phys. Res. B **59/60**, 1378 (1991).
  - [14] A. Gras-Martí *et al.*, Comp. Mat. Sci. **3**, 413 (1995).
  - [15] K. Nordlund, J. Keinonen, and T. Mattila, Phys. Rev. Lett. **77**, 699 (1996).
  - [16] J. Tersoff, Phys. Rev. B **37**, 6991 (1988).
  - [17] J. Tersoff, Phys. Rev. Lett. **61**, 2879 (1988).
  - [18] R. Smith and D. E. Harrison, Jr., Computers in Physics **Sep/Oct 1989**, 68 (1989).
  - [19] M. P. Allen and D. J. Tildesley, *Computer Simulation of Liquids* (Oxford University Press, Oxford, England, 1989).
  - [20] K. Nordlund, Comp. Mat. Sci. **3**, 448 (1995).
  - [21] J. F. Ziegler, J. P. Biersack, and U. Littmark, *The Stopping and Range of Ions in Matter* (Pergamon, New York, 1985).
  - [22] P. A. Thrower and R. M. Mayer, Phys. Stat. Sol. (a) **47**, 11 (1978).
  - [23] R. B. Capaz, K. Cho, and J. D. Joannopoulos, Phys. Rev. Lett. **75**, 1811 (1995).
  - [24] A. Selloni, P. Carnevali, E. Tosatti, and C. D. Chen, Phys. Rev. B **31**, 2602 (1985).
  - [25] J. Tersoff and D. R. Hamann, Phys. Rev. Lett. **50**, 1998 (1983).
  - [26] We use the parametrization for LDA exchange-correlation term by J. Perdew and A. Zunger, Phys. Rev. B **23**, 5048 (1981).
  - [27] D. Vanderbilt, Phys. Rev. B **41**, 7892 (1990), K. Laasonen *et al.*, Phys. Rev. B **47**, 10142 (1993).
  - [28] H. J. Monkhorst and J. D. Pack, Phys. Rev. B **13**, 5188 (1976).
  - [29] N. Troullier and J. L. Martins, Phys. Rev. B **43**, 1993 (1991).
  - [30] H. Maeta, T. Iwata, and S. Okuda, Phys. Lett. **53A**, 295 (1975).
  - [31] J. C. Grossman, L. Mitas, and K. Raghavachari, Phys. Rev. Lett. **75**, 3870 (1995).
  - [32] N. A. Marks *et al.*, Phys. Rev. Lett. **76**, 768 (1996).
  - [33] G. E. Scuseria, Science **271**, 943 (1996).
  - [34] An MPEG animation of the formation of the D3 defect is available on the World Wide Web in <http://beam.helsinki.fi/~knordlun/graphite.html>.